

# Chirped excitation of optically dense inhomogeneously broadened media using $\text{Eu}^{3+}:\text{Y}_2\text{SiO}_5$

Todd L. Harris, Mingzhen Tian, and W. Randall Babbitt

*Spectrum Lab, Montana State University, Bozeman, Montana 59717-3510*

Geoffrey W. Burr, John A. Hoffnagle, and C. Michael Jefferson

*IBM Almaden Research Center, 650 Harry Road, San Jose, California 95120-6099*

Received April 21, 2003; revised manuscript received October 10, 2003; accepted December 3, 2003

We describe experimentally accessible diagnostics for the excitation of optically dense frequency-selective media by linear frequency-chirped pulses using a sensitive pump-probe technique on the  ${}^7F_0$  to  ${}^5D_0$  transitions of 1.0%  $\text{Eu}^{3+}:\text{Y}_2\text{SiO}_5$ . Distinct features within a transmitted cw probe pulse are used to identify the combination of linear chirp rate and optical power needed to produce an average Bloch-vector rotation of  $90^\circ$ . The resulting superposition state is thus an equal mixture of the ground and excited states on average. We find experimentally a linear relationship between the applied chirp-pulse intensity and chirp rate required to produce this half-inversion, a conclusion supported by both analytical calculations made using a Landau-Zener approach, and detailed computer simulations using the Maxwell-Bloch model. The numerical simulations predict experimentally observed phenomena such as the reshaping of probe pulses by stimulated emission or absorption. Finally, we quantify the relationship between chirp rate and optical power for half-inversion as a function of the optical density of the medium. The pump-probe experimental techniques and simulation analysis techniques developed here can be extended to produce an arbitrary mixture of ground and excited states, on average, in media spanning a wide range of optical density. Preparation of such media by chirped pulses for applications in quantum computing, photon-echo-based time-domain storage, and signal processing will be aided by these techniques. © 2004 Optical Society of America

OCIS codes: 060.5060, 300.6240, 160.5690, 000.4430.

## 1. INTRODUCTION

Optical coherent transients (OCTs) have been used extensively for coherent spectroscopy of optical materials<sup>1</sup> and have been proposed and demonstrated as the basis for storage and processing of both classical and quantum information. In particular, Levenson<sup>2</sup> and Mossberg<sup>3</sup> independently proposed that a hole-burning material such as  $\text{Eu}^{3+}:\text{Y}_2\text{SiO}_5$  (Eu:YSO) could record the product of the Fourier transforms of three pulses: the two optical pulses (reference and data) used to write a spectral grating, and the recall pulse.<sup>2</sup> It was originally proposed that the reference and recall pulses should be brief tone bursts, ideally resembling a delta function with constant power over the data spectrum,<sup>3</sup> in order to reproduce a data pulse with the highest fidelity. It was soon realized that, although such a pair of brief reference and recall pulses can, in principle, accurately reproduce stored data, the optical power available from laser sources of the appropriate wavelength is typically too low. Practical sources often cannot provide enough power in a brief pulse to pump a significant fraction of the medium from the ground state to the excited state over the wide bandwidth of the data to be stored and retrieved. Linear frequency-chirped<sup>4</sup> optical pulses have been proposed<sup>5</sup> and demonstrated<sup>6</sup> as both a practical substitute for brief reference pulses in power-limited circumstances and as

an enabling component of novel processor functions in OCT-based devices.

Many demonstrations of optical pulse compression,<sup>6</sup> data storage,<sup>7</sup> bit-rate conversion and time reversal,<sup>8</sup> and true-time delay<sup>9</sup> have been conducted using chirped pulses. However, propagation effects in optically dense media,<sup>10</sup> ion-ion effects such as excitation-induced dephasing,<sup>11</sup> and nonuniform transverse laser intensity profile all complicate optimization of OCT devices, regardless of excitation-pulse format. Brief pulse excitation of frequency-selective media having a wide range of optical density, and reshaping of such pulses upon propagation through these media, have been investigated extensively both theoretically and experimentally.<sup>12</sup> Analogous studies using linear frequency-chirped pulses are comparatively lacking in the literature.

The objective of this work was to study how a chirp optically pumps the  ${}^7F_0$  to  ${}^5D_0$  transitions in Eu:YSO. In particular, we wished to determine the chirp rate and optical power needed to produce, on average, an equal superposition of the ground and excited states in the media. A pulse that creates such a superposition would be analogous to a pulse having an area<sup>13</sup> of  $\pi/2$  except that the resulting half-inversion could be produced over a large bandwidth when using such chirped pulses. In this paper, we describe an experimentally accessible diagnostic

for excitation with chirps. First, we pump the media from the ground state with a chirp of interest, then we use the reshaping of a brief probe pulse to gauge the average population inversion produced by the chirp. Oscilloscope recordings of several such pump-probe experiments are shown in Fig. 1; the transmitted intensity of the chirped pump and brief probe pulse, and the photon echo that they generate, are shown on separate scales.

Figure 1 shows that as the optical power in the chirp is increased (with both chirp rate and bandwidth fixed), the overall slope of the transmitted probe changes from positive to zero to negative. We interpret these three regimes as corresponding to less than a half-inversion, half-inversion, and greater than half-inversion, respectively, as averaged over the length of the optically dense media, Gaussian spatial profile of the laser beam, and bandwidth of the probe pulse. The upward trend in transmitted

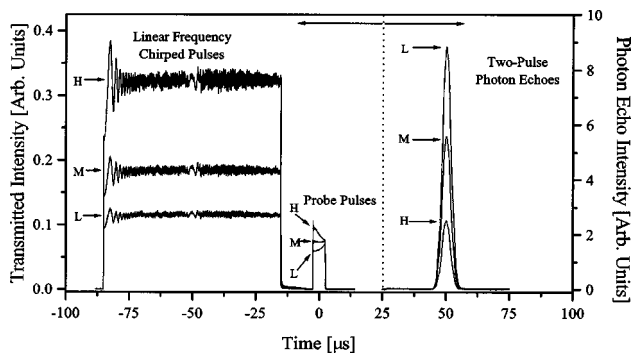


Fig. 1. Oscilloscope traces of transmitted chirped-pump/cw-probe pulse pairs and the resulting photon echo; each is an average of 32 shots. The chirp rate is fixed. The shape of the transmitted probe pulse indicates the degree of inversion created by the chirped pulse. “H” indicates the highest applied chirp power, and “L” is the lowest.

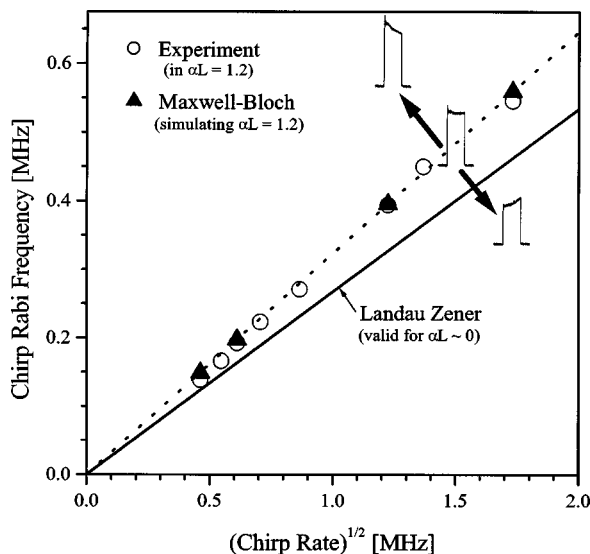


Fig. 2. Combinations of chirp Rabi frequency and root chirp rate that created a half-inversion in experiment (open circles) and in simulation (solid triangles). The dotted line is a linear fit to the simulation results. The solid line is the low optical-density limit predicted by Landau-Zener theory. The slopes of lines on this graph are dimensionless-coupling strengths,  $\Phi$ .

pulse intensity in the first regime corresponds to continued optical pumping and absorption from the incident field. The decreasing intensity of the transmitted pulse in the third regime results from net stimulated emission due to the greater than half-inversion produced by the most intense of the three chirps. Thus the middle regime corresponds to a half-inversion, where absorption and stimulated emission are balanced on average throughout the optically dense medium, allowing the probe pulse to pass through nearly unperturbed. This interpretation of the shape of the transmitted probe pulse provides a simple diagnostic of the degree of media inversion.

Using this pump-probe technique, we were able to identify experimentally the combinations of chirp rate and applied optical chirp intensity required to create a half-inversion. The open circles in Fig. 2 summarize a series of experiments where the applied chirp power necessary to create a half-inversion, at a variety of applied chirp rates, was indicated by the probe pulse. These results are plotted in terms of the Rabi frequency (which is proportional to the applied electric field) of the applied chirp and the square root of the chirp rate. This figure shows that, when a half-inversion has been created, a linear relationship exists between the applied chirp intensity and chirp rate. Transmitted probe pulses have been inset to illustrate the reshaping that occurs when the combination of chirp power and chirp rate differs from that required to create a half-inversion. In the remainder of this paper, we support this interpretation using a combination of experiments, numerical simulations based on the coupled Maxwell-Bloch equations, and analytical calculations based on Landau-Zener theory. The experimental diagnostics and simulation analysis described here will aid in the precision preparation of frequency-selective media for applications such as quantum computation<sup>14,15</sup> and OCT-based memory and signal processing.

## 2. BACKGROUND

Landau and Zener observed<sup>16,17</sup> that there is an exact, analytic solution to the two-level Schrödinger equation for a system having an interaction potential of constant amplitude and a resonance condition between the two levels that varies linearly with time. It was later realized that this problem is mathematically identical to that of driving a two-level system whose energy levels are constant in time with a harmonic-excitation field whose frequency is swept linearly in time. More recently, Vitinov and Garraway<sup>18</sup> presented a detailed discussion of approximate solutions to the Landau-Zener problem for the case of finite-duration excitations, such as chirped laser pulses. The Landau-Zener model is attractive because it has been used to derive simple, analytic expressions that predict the transition probability of an atom under chirped excitation, but it is important to recognize that the theory describes a highly idealized physical system. Population and coherence decay are neglected, so the treatment is valid only for time intervals that are short compared with the dephasing time of the material being used. Because the starting point is the two-level Schrödinger equation, Landau-Zener theory is applied here, assuming that there is a single average transition dipole

moment  $\mu_{21}$  that effectively describes the entire sample. However, our experiments use a sample that is optically dense, has nine hyperfine transitions per isotope, and is excited by a nonuniform transverse laser intensity profile.

Subject to these qualifications, Landau–Zener theory predicts transition probabilities for chirped excitation of a two-level system initially in the ground state. Vitanov and Garraway have solved this problem explicitly in terms of a “scaled dimensionless coupling strength,” which is a fundamental scaling parameter for chirped excitation of a two-level system:

$$\Phi \equiv \frac{\Omega_0}{(B_c/\tau_c)^{1/2}}. \quad (1)$$

Here  $\Omega_0 = \mu_{21}E_0/\hbar$  is the Rabi frequency of the chirped pulse in units of  $s^{-1}$  (here  $\Omega_0$  should be thought of as the effective electric field  $E_0$ , normalized by the dipole moment);  $B_c/\tau_c$  is the experimental chirp rate in units of  $s^{-2}$ , where  $B_c$  and  $\tau_c$  are the chirp bandwidth in hertz and chirp duration in seconds, respectively.<sup>19</sup> Therefore the dimensionless coupling strength squared,  $\Phi^2$ , is proportional to the ratio of the applied chirp-pulse intensity to the applied chirp rate.

If the time–bandwidth of the chirp is large, then for atoms whose resonance frequencies are near the center frequency of the chirp, the original Landau–Zener formula for transition probability  $P$  to the excited state in terms of the dimensionless coupling strength applies:

$$P = 1 - \exp[-(\pi\Phi)^2]. \quad (2)$$

For comparison with experimental data and benchmarking of our Maxwell–Bloch simulations in later sections, we write Eq. (2) in terms of the component of the optical Bloch vector<sup>20</sup> that represents material inversion  $r_3$  (the normalized difference between excited and ground-state populations) by substituting  $P = (r_3 + 1)/2$  into Eq. (2) to obtain

$$r_3(\Phi) = 1 - 2 \exp[-(\pi\Phi)^2]. \quad (3)$$

Because we are interested in the combination of applied chirp-pulse intensity and chirp rate to obtain a particular media inversion, we solve Eq. (3) for  $\Phi$  to obtain

$$\Phi(r_3) = \frac{1}{\pi} \sqrt{\ln\left(\frac{2}{1-r_3}\right)}. \quad (4)$$

This indicates that the ratio of Rabi frequency of the applied chirp to square root of the chirp rate determines media inversion. The ratio between  $\Omega_0$  and  $(B_c/\tau_c)^{1/2}$  predicted by Landau–Zener for a chirp to prepare a half-inverted population ( $P = 1/2$  or  $r_3 = 0$ ) is then

$$\Phi(0) = 0.265. \quad (5)$$

This result is plotted in Fig. 2 as a solid line that represents the dimensionless-coupling strength required to produce a half-inversion in the low-optical-density limit. For an inversion other than the half-inversion of primary interest here, the quotient of Rabi frequency and root chirp rate will be different, thus producing a line in Fig. 2 of a different slope and representing the low-optical-density bound for that inversion.

### 3. EXPERIMENTAL METHODS AND APPARATUS

The Eu:YSO spectral hole-burning material has been studied extensively for persistent, time-domain optical memory.<sup>21–24</sup> By design, it provides both persistent storage (several days under cryogenic conditions) in the ground-state hyperfine levels of the  $\text{Eu}^{3+}$  ions and a long coherence lifetime due to negligible dephasing of the  $\text{Eu}^{3+}$  by nuclear spin flips of the  $\text{Y}_2\text{SiO}_5$  host constituents. A crystal of nominal 1.0% Eu concentration was obtained from Scientific Materials Corporation, Bozeman, Montana. The crystal was oriented<sup>25–27</sup> with its  $D_1$  axis parallel with the linearly polarized laser and its  $b$  axis parallel with the laser propagation direction. The crystal was 2.6 mm thick, with  $\alpha_0 = 4.6 \text{ cm}^{-1}$  for a peak absorption length of  $\alpha_0 L = 1.2 \pm 0.1$ . Experiments were conducted on crystallographic Site 1, located at 579.879 nm, with the crystal at a temperature of  $4.0 \pm 0.2 \text{ K}$  in an Oxford Instruments model CF1204 He cryostat. Under these conditions, the coherence lifetime,  $T_2$ , was previously measured to be  $\sim 1.1 \text{ ms}$  for 1% dopant concentration, and the upper-state lifetime,  $T_1$ , was  $\sim 2.0 \text{ ms}$ .<sup>24</sup>

A schematic of the laser systems and the experimental apparatus is shown in Fig. 3. A Coherent I-200 argon laser at 514 nm with 7-W nominal power pumped an extensively modified Coherent CR699-29 dye laser, which was

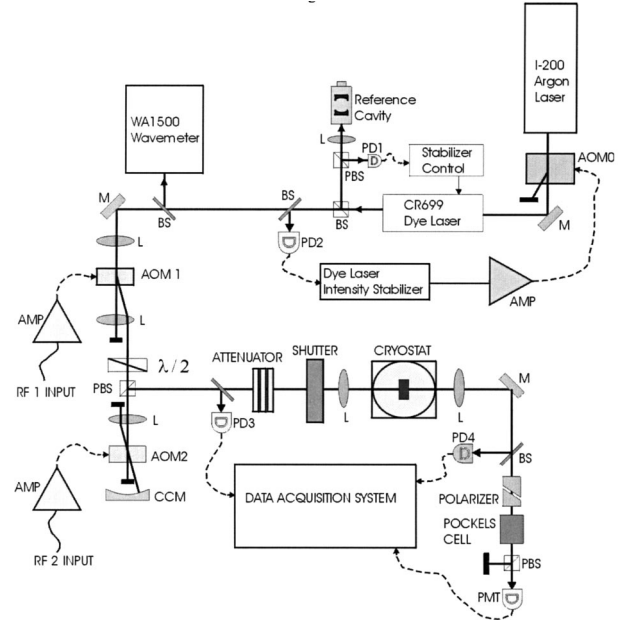


Fig. 3. Schematic of the experimental apparatus. The dye laser was stabilized both in intensity and frequency. An acousto-optic modulator, AOM 1, was used to gate the laser beam. AOM 2 was used in a double-pass configuration to impress linear frequency chirps and arbitrary frequency offsets on the pulses from AOM 1. The laser was then focused into the  $\text{Eu}^{3+}:\text{Y}_2\text{SiO}_5$  crystal residing in the cryostat. The laser pulses before and after the cryostat were recorded with fast silicon photodiodes (PD). A photomultiplier tube (PMT), protected from overload by a Pockels cell optical gate, measured the photon echoes. In the figure, M labels mirrors, L labels lenses, CCM indicates the concave mirror, BS labels beam splitters,  $\lambda/2$  labels half-wave plates, PBS labels polarizing beam splitters, and AMP labels radio-frequency amplifiers used to drive the acousto-optic modulators.

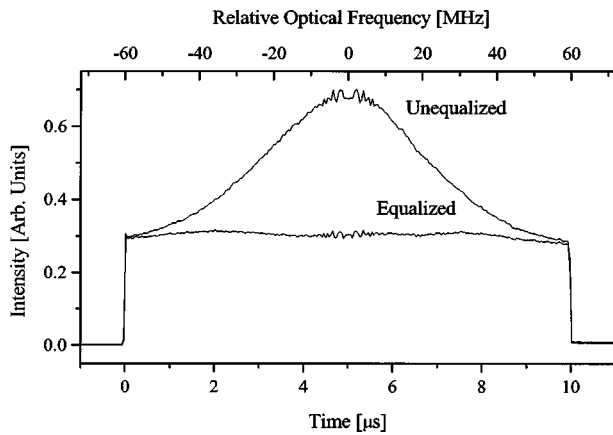


Fig. 4. Effect of compensating the transfer function of AOM2. The upper trace is the intensity of an unequalized chirp of 120-MHz optical bandwidth generated by AOM2, as measured by PD3. The intensity rolloff is due to the modulator transfer function. The lower trace is the result of predistorting the RF drive signal amplitude to compensate for the modulator transfer function, which produces a constant-intensity chirped pulse. The residual intensity ripple that is symmetric about the center of the chirp is an artifact caused by low digital sampling resolution in the construction of the RF chirp waveform. This artifact is evident in the transmitted chirps in Fig. 1.

stabilized in both power and frequency. The dye laser's power was stabilized under closed loop control. Photodiode PD-1 monitored the power before AOM-1, and the RF drive power applied to AOM-0 was controlled by a PID feedback circuit slaved to the resulting photocurrent. Using the zero-order beam from AOM-0 to pump the dye laser minimized pump-beam distortion and maximized use of the available pump power. Factors that contributed to residual intensity fluctuations at the sample were vignetting of the beam at various apertures in the beam path, etalon effects due to the uncoated crystal and windows in the cryostat, and scattered light at locations downstream from the intensity monitor. The laser power at the sample was typically controlled to better than 1% rms over millisecond durations.

To eliminate frequency jitter and thus narrow the linewidth, the dye laser was locked to a high-finesse optical cavity whose linewidth was  $\sim 100$  kHz. Using the Pound-Drever-Hall technique,<sup>28</sup> the laser-frequency fluctuations were canceled by a combination of a high-speed intracavity electro-optic modulator (Gsanger PM-25) and feedback to the dye-laser internal piezo-mirror and galvo circuits. With respect to the reference cavity, the linewidth of the laser was estimated to be less than 1 kHz by comparing the in-lock and out-of-lock stabilizer error signals.

Chirped optical pulses having high on/off contrast ratio were generated first by gating the cw laser with an acousto-optic modulator (AOM-1; Crystal Technology model 3200-121) and then by impressing the chirp on the resulting pulse using an identical modulator (AOM-2) in double-pass configuration to compensate frequency-dependent beam steer. The chirps applied to AOM-2 were generated by an Analogic model 2045 waveform synthesizer with 8-bit resolution and an 800 megasamples/second (MS/s) data rate. The data points that generated the RF chirps were amplitude compensated and predis-

torted using the inverse of the transfer function of the modulator, as measured off line, resulting in power flatness of several percent over the practical chirp bandwidth, up to 120 MHz. The powers of both the unequalized and equalized chirps as detected by photodiode PD1 just before the cryostat are shown in Fig. 4. Residual high-frequency ripple in the chirp power is deterministic and due to insufficient resolution in the digital-to-analog reconstruction of the chirp waveform. It is observable in both the optical pulses that are applied to the crystal and those that were transmitted.

A tunable RF synthesizer (HP 8656B) and fast GaAs RF switch generated the cw tone-burst pulses used to probe the population inversion created by the chirped pulse. The RF chirp and cw probe pulses were summed with a power combiner before being amplified and applied to AOM-2. Computer-programmed pulse generators (SRS DG535) controlled the timing of the experiment.

For each experiment, the temporal shapes of the chirped and cw probe pulses before the crystal were recorded. A beam splitter located before the cryostat deflected a few percent of the optical power to a 1-GHz Si PIN photodiode (PD1). The signal from PD1 was amplified and captured on a Tektronix model DSA 602 digitizing signal analyzer at a rate of 100 MS/s. We thus ensured that the incident probe pulses had square-power envelopes. Transmitted excitation pulses and photon echoes were recorded by the digital signal analyzer. The high-power transmitted excitation pulses were detected by a second fast Si PIN photodiode (PD2). The low-power two-pulse photon echoes were detected by a Hamamatsu R928 photomultiplier tube, which was protected from the high-power excitation pulses by a Pockels cell and polarizing beam splitter (PBS).

The Gaussian-profile laser beam was focused in the sample to an average  $1/e^2$  waist diameter,  $d_0$ , of  $95 \pm 10 \mu\text{m}$ , as measured with a Photon, Inc., model 1180 Beam Scan. The beam diameter was constant to within  $5 \mu\text{m}$  over the thickness of the sample. To determine the optical power needed to generate the cw probe pulse, we used nutation signals in the standard way<sup>25,29</sup> to measure the projection of the effective dipole moment,  $\mu_{21}$ , along  $D_1$  for Site 1 of our crystal. We define  $\mu_{21}$  to be an average of the transition dipole moments for all nine hyperfine transitions of  ${}^7F_0$  to  ${}^5D_0$  in both  ${}^{151}\text{Eu}$  and  ${}^{153}\text{Eu}$  in these mixed isotope samples. Our measured value of this effective dipole moment is  $1.56 \times 10^{-21}$  esu-cm, and it is consistent with a previously measured value.<sup>30</sup> This measurement cannot be made in this material system without a laser whose coherence time is much longer than the time that the cw nutation signal damps completely (10–100  $\mu\text{s}$ , typically).

The value of the dipole moment is related to the Rabi frequency,  $\Omega_0$ , and to the laser intensity,  $I$ , by

$$I = \left( \frac{p}{A_{\text{TH}}} \right) = \frac{cn}{8\pi} \left| \frac{\hbar\Omega_0}{\mu_{21}} \right|^2, \quad (6)$$

where  $n = 1.8$  is the mean refractive index of YSO,  $A_{\text{TH}} = \pi d_0^2/8$  is the equivalent "top-hat" area of a Gaussian



beam<sup>31</sup> for a  $1/e^2$  waist diameter  $d_0$ , and  $p = A_{\text{TH}}I$  is the optical power inside the crystal. Solving for  $\Omega_0$  yields

$$\Omega_0 = \left( \frac{8\pi\mu_{21}^2}{cn\hbar^2} \right)^{1/2} \left( \frac{p}{A_{\text{TH}}} \right)^{1/2} \equiv C_{\text{Rabi}}\sqrt{I}. \quad (7)$$

The effective average Rabi frequency coefficient  $C_{\text{Rabi}}$  for the sample and orientation chosen has a value of  $215 \pm 5 \text{ Hz/W}^{1/2}/\text{m}$ . This quantity will be used implicitly throughout the remainder of the paper to calculate Rabi frequencies from measured optical powers.

#### 4. MAXWELL–BLOCH SIMULATION

The finite Landau–Zener formalism of Vitanov and Garraway introduced above is valid only for the case of a single isolated two-level system excited by a high time–bandwidth product linear frequency-chirped optical pulse. Thus the analytic expressions generated by this theory are only valid in certain restrictive asymptotic regimes and for the case of low optical density. The behavior of the system that we have studied experimentally can be more properly described by numerically integrating the coupled Maxwell–Bloch equations.<sup>10</sup> This approach combines the optical Bloch equations (to model the coherence and population dynamics of an inhomogeneously broadened ensemble of two-level systems) with Maxwell’s wave equation (to model propagation effects through the optically dense media). Our implementation uses the “conventional” Maxwell–Bloch model (described in detail in Section 3 of Ref. 32), which does not include complicating effects as excitation-induced dephasing or nonuniform transverse laser profile. The computer simulations of our pump–probe experiments assume plane wave, nearly monochromatic optical excitation of two-level atoms. Their application to the excitation of Eu:YSO, containing multiple ground- and excited-state hyperfine levels, by optical beams with Gaussian profiles is approximate. Despite this, we obtain excellent agreement between simulations and experiment and also useful intuition into the experimental results.

In order to model the pump–probe experiments, we define the complex Rabi frequency  $\Omega_{r,i}(t)$  at each time step as initial conditions and solve the system of coupled Maxwell–Bloch equations to determine the Bloch-vector components  $r_1$ ,  $r_2$ , and  $r_3$  at each layer of the medium. The simulated medium was divided into 125 layers along the laser propagation direction  $z$ , each with absorption length  $\alpha \cdot \delta z = 0.08$ , providing a total absorption length of  $\alpha L = 10.0$ . The simulated pulses were propagated through this medium and arrays of the values of the complex electric field  $\Omega_{r,i}(z, t)$ , and Bloch-vector components  $r_{1,2,3}(z, \Delta)$  were saved from every layer. Thus from a single simulation, sufficient information was captured to model media of optical densities ranging from the density of the first layer up to the density of all layers combined. For example, the electric field emitted by the  $j$ th layer is the same as that emitted by a medium with an absorption length  $j \cdot \alpha \cdot \delta z$ . The  $r_3$  component of the Bloch vector could be averaged from  $z = 0$  to  $z = j \cdot \delta z$  to obtain the average inversion in a medium of absorption length  $j \cdot \alpha \cdot \delta z$ .

#### 5. RESULTS AND DISCUSSION

The results of experiment, numerical simulation, and analytic theory will now be compared. We will show that Maxwell–Bloch simulations strongly support the use of the transmitted probe pulse to gauge average media inversion and validate the interpretation that a probe pulse having zero overall slope indicates a half-inversion, on average, through the optical density of the media and across the nonuniform laser profile. We have seen that Landau–Zener theory predicts the linear relationship between the optical intensity and chirp rate that creates a constant inversion in the zero optical-density limit. Maxwell–Bloch simulations also support this observation and agree well with our data for the conditions that produce half-inversion. The numerical accuracy of the Maxwell–Bloch simulator is found to be in good agreement with predictions of Landau–Zener in the low optical-density limit, as expected. Finally, we use the Maxwell–Bloch modeling to extend the results of Landau–Zener for arbitrary inversion to the case of optically dense media.

##### A. Probe-Pulse Diagnostic of Inversion

We found experimentally that, when the optical power of the applied chirp was varied, the shape of the subsequent probe pulse changed as well, as shown in Fig. 1. For a chirp pulse of high optical power, the transmitted probe pulse had an initially high power that decayed in time. Conversely, for a chirp pulse of low optical power, the probe-pulse power increased in time. The transmitted power of the probe pulse could be made essentially constant by choosing a particular value of the chirp-pulse optical power, as shown in the middle trace of Fig. 1. We hypothesized that such a probe pulse indicated a half-inversion on average through the media and that the incident probe pulse caused no net stimulated absorption or emission.

To test this hypothesis, we simulated the pulse sequence in Fig. 1 using the same chirp rate and the same cw probe-pulse intensity and duration as in the experiment; an example of such simulation results is shown in Fig. 5. The dotted trace in Fig. 5(a) is the relative intensity incident at  $z = 0$ , and the solid trace is the simulated optical intensity transmitted through the first 15 layers, corresponding to our experimental absorption length of 1.2. The first pulse is a chirp, and the second is a brief probe pulse; the inset trace shows that its overall slope is nearly zero. Note that the simulation also predicts the two-pulse photon echo. In computing the time-domain response of the media to the applied pulse sequence, the simulator also calculates the inversion as a function of frequency created by the pulse sequence. Figure 5(b) shows the inversion as a function of detuning  $r_3(\Delta)$  immediately prior to the probe pulse and averaged over the absorption length of our crystal,  $\alpha L = 1.2$ . This “density-averaged” inversion is slightly less than 0 at the center frequency of the chirp ( $\Delta = 0$ ), indicating just less than half-inversion  $\langle r_3 \rangle = 0$  at the probe-pulse frequency. It should be noted that the combination of the slightly positive slope of the probe pulse and the slightly less than half-inversion is consistent with our hypothesis.

To further test our hypothesis, the simulator was run multiple times using a fine grid of chirp-pulse Rabi frequencies and chirp rates spanning the experimental conditions so that the combinations that create half-inversion could be determined by interpolation. Representative results of transmitted probe pulses are shown in Fig. 6(a) from simulations using the same chirp rate but different chirp Rabi frequencies as in Fig. 1. The density-averaged inversions  $\langle r_3 \rangle$  created by the chirp pulses are shown in Fig. 6(b). The complete set of simulations shown span the region where half-inversion occurs. When the chirp Rabi frequency is too high, the probe pulse (H) has a negative overall slope as in the experiments, and for this case, we note that  $\langle r_3 \rangle > 0$ . Conversely, when the chirp Rabi frequency is too low, the probe pulse (L) has a positive slope and  $\langle r_3 \rangle < 0$ .

We fit the envelopes of the probe pulses with straight lines, as in the dotted lines in Fig. 6(a), to estimate the overall slope of the probe pulse. The density-averaged inversions in Fig. 6(b) were further averaged over a 1-MHz bandwidth centered at  $\Delta = 0$  to estimate the inversion over the full bandwidth of the probe pulse. The slopes of many such fitted lines and the corresponding average inversions are plotted in Fig. 6(c) and labeled with the dimensionless coupling strength of the corresponding

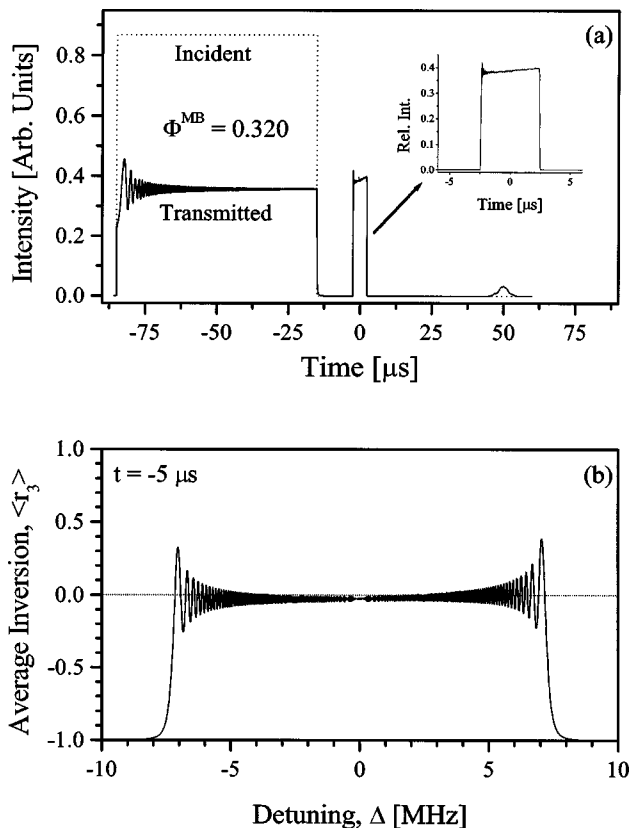


Fig. 5. Maxwell-Bloch simulation of a pump-probe experiments with  $\alpha L = 1.20$ , analogous to those in Fig. 1. The dotted trace in the upper panel is the incident intensity, and the solid trace is the intensity after transmission. The bottom panel shows the average inversion,  $\langle r_3 \rangle$ , as a function of detuning following the chirp. The transmitted chirp exhibited nutation and created slightly less than a half-inversion, as indicated by both the transmitted probe-pulse slope and  $\langle r_3 \rangle$ .

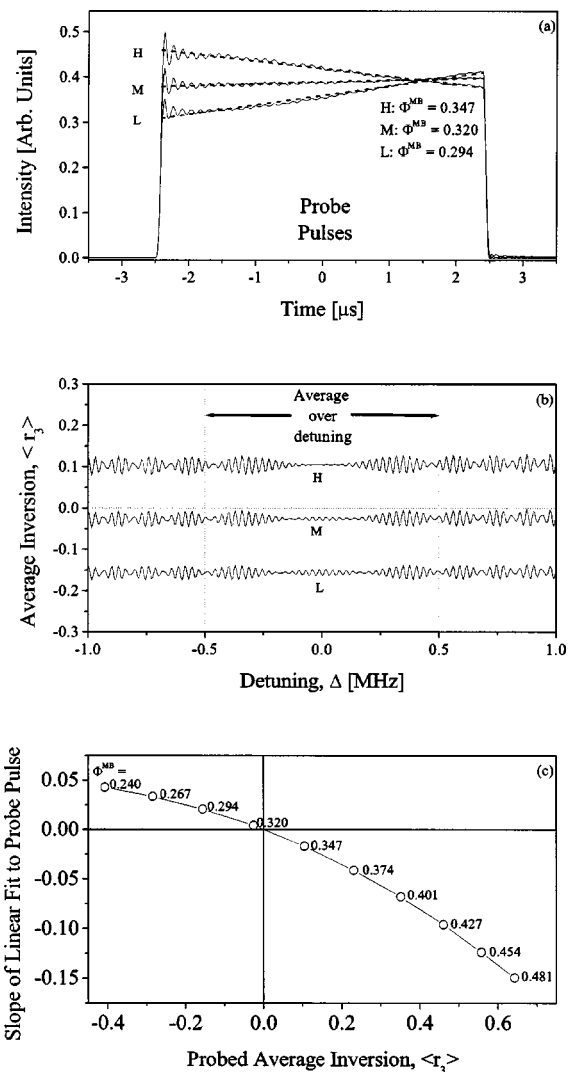


Fig. 6. Graphical representation of the analysis associating the probe-pulse shape with media inversion. Subplot (a) shows several simulated probe pulses for experimental conditions of Fig. 1. Each pulse has been fit with a straight line between its rising and falling edges. Subplot (b) shows the inversion, averaged over optical density, through which each probe pulse was transmitted. Vertical lines at  $\Delta = \pm 0.5$  MHz indicate the detuning range over which the inversion was averaged. The slopes of the lines fit to the probe pulses are plotted versus the corresponding average inversion in subplot (c); the dimensionless coupling strength,  $\Phi$ , used to generate each inversion labels the points. The curve fit to these data shows that the probe slope is zero at  $\langle r_3 \rangle = 0$ .

chirp. Note that the curve fit to this data set indicates that zero probe-pulse slope occurs at  $\langle r_3 \rangle = 0$ , which establishes that a flat probe-pulse shape indicates half-inversion of the media.

In order to interpolate the dimensionless-coupling strengths required for a half-inversion from the set of discrete values used in simulation, we fitted both the probe slope and the average inversion as functions of dimensionless-coupling strength with *ad hoc* polynomials and found their roots. We performed identical analyses on all the simulations, which span absorption lengths from  $\alpha L = 0$  to 10 and several chirp rates. The dimensionless-coupling strength at which half-inversion

was achieved and at which the probe-pulse slope was zero differed by only 0.7% rms over the entire set of simulations. This establishes that a probe-pulse slope of zero is an indication that a half-inversion has been achieved within the approximations of our simulator. Finally, for all chirp rates simulated, the aggregate dimensionless coupling strength for half-inversion in  $\alpha L = 1.2$  was  $\Phi_{1/2}^{\text{MB}} = 0.322$ .

### B. Media Inversion by Chirps

We have now established our association of the flat probe pulse with a half-inversion on average through the media. In Fig. 2, we showed experimentally that the combination of chirp Rabi frequency and square-root chirp rate required to create a half-inversion as determined by the probe-pulse technique fell on a straight line. For a given chirp rate, we calculated the dimensionless coupling strength from Eq. (1) by measuring the applied optical power of the chirp, using the Rabi-frequency coefficient,  $C_{\text{Rabi}}$ , from Eq. (7). We thus obtain the experimental dimensionless-coupling strength for half-inversion in our crystal ( $\alpha L = 1.2 \pm 0.1$ ):

$$\Phi_{1/2}^{\text{EX}} = \frac{\Omega_c}{(B_c/\tau_c)^{1/2}} = 0.32 \pm 0.01, \quad (8)$$

in good agreement with our simulation,  $\Phi_{1/2}^{\text{MB}} = 0.322$ , and larger than the Landau-Zener result [Eq. (5)],  $\Phi_{1/2}^{\text{LZ}} = 0.265$ , which sets the low optical-density limit. The dotted line is a linear fit to the Rabi frequency versus root chirp rate required for half-inversion (solid triangles) obtained from the analyses of the Maxwell-Bloch simulations for the various chirp rates simulated. The

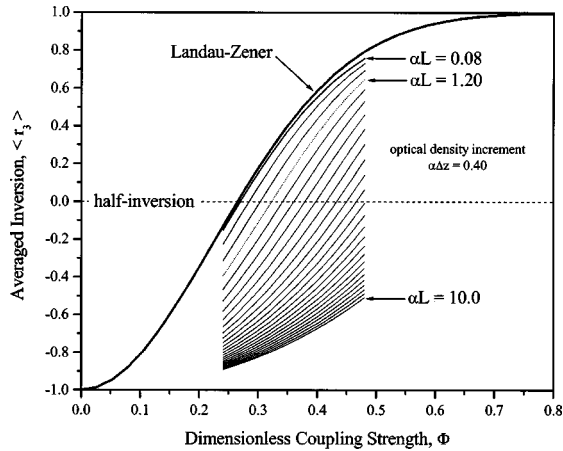


Fig. 7. Calculated media inversion as a function of dimensionless-coupling strength,  $\Phi$ , for a wide range of absorption lengths. The uppermost curve is the Landau-Zener prediction, valid for  $\alpha L = 0$ . The predictions of the Maxwell-Bloch simulations are shown as a family of curves. Each represents the inversion,  $r_3$ , averaged over  $\alpha L$  and over a bandwidth,  $\Delta = \pm 0.5$  MHz, about the center of the chirp. The uppermost of these is from the first slice of media, representing  $\alpha L = 0.08$ . The remaining simulation curves are for  $\alpha L$  ranging from 0.40 to 10.0 in increments of 0.40. The curve for  $\alpha L = 1.2$  predicts the average inversion for the same optical density as the experimentally studied sample. The intersection of each curve with the dotted horizontal line at  $\langle r_3 \rangle = 0$  indicates the dimensionless-coupling strength required to create a half-inversion.

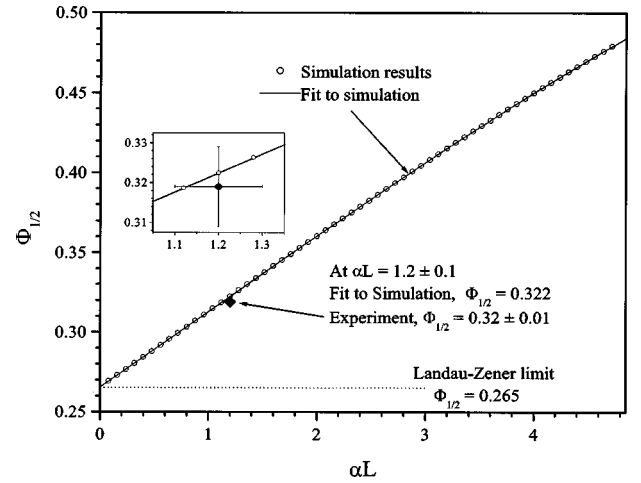


Fig. 8. Dimensionless-coupling strength  $s$  required to create a half-inversion are plotted as a function of absorption length. The solid line is a polynomial fit to these results. The solid diamond represents the dimensionless-coupling strength experimentally found to create a half-inversion in  $\alpha L = 1.2$ , which was calculated from the slope of the line in Fig. 4 as described in the text.

Landau-Zener bound over the full range of chirp rates is illustrated with a solid line. The slopes of the lines on this plot are thus the dimensionless coupling strength for half-inversion.

We now investigate the question of what Maxwell-Bloch predicts for absorption lengths other than  $\alpha L = 1.20$ . Figure 7 plots a fit to the average inversion versus dimensionless coupling strength for the simulation data points shown in Fig. 6(c). That curve is labeled as  $\alpha L = 1.20$ . In addition, a family of such curves are shown for  $\alpha L = 0.08$  and from  $\alpha L = 0.40$  to 10.0 in increments of 0.40. These represent the dimensionless-coupling strength required to generate arbitrary inversions in media of optical density for the values simulated. Equation (3) is plotted at the far left of Fig. 7 and shows that the Maxwell-Bloch simulations agree well with Landau-Zener theory in the low optical-density limit, as expected.

Figure 8 shows a correction to the Landau-Zener prediction for half-inversion in media of nonzero optical density. The roots of the curves in Fig. 7 are the dimensionless coupling strengths to achieve half-inversion. These roots are plotted in Fig. 8 versus the subset of simulated optical densities in which half-inversion was achieved. The solid curve is an *ad hoc* polynomial fit which approaches the Landau-Zener prediction at  $\alpha L = 0$  as expected. These analyses could be extended to predict the dimensionless coupling strength required to create any other desired media inversion.

### C. Limits of Validity

We explored the range of validity of the transmitted probe-pulse technique. For the experimental parameters chosen for this study, the probe pulse only substantially interrogates a narrow frequency interval,  $\sim 200$  kHz, at the center of a spectrally broad, 15-MHz, excited ensemble of ions. We used AOMs 1 and 2 to successively shorten the duration of a chirp of fixed chirp rate, thus



proportionally narrowing its bandwidth. We found that when the bandwidth of the chirp became comparable to that of the probe, the probe pulse developed oscillations that made it impossible to define an overall slope and therefore made the probe useless as an indicator of media inversion. Under these conditions, the chirp had a quite small time-bandwidth product and therefore acted more like a transform-limited pulse.

Finally, because the pump-probe technique is dependent on the relative ground- and excited-state populations, the pulse sequence must be completed within a time scale that is small compared with the material population relaxation. This is easily satisfied in this case because  $T_1 \sim 2$  ms for  $\text{Eu}^{3+}$  ions in Site 1, and each experiment was completed within 100  $\mu\text{s}$ . The experiments were also completed well within the coherence lifetime of the material. The pump-probe experiments are expected to be insensitive to coherence loss that is not due to population decay because they only rely on individual ions absorbing or emitting coherently with the driving field, not on ensembles of ions being coherent with one another. This hypothesis was supported by Maxwell-Bloch simulations in which the Bloch-vector components  $r_1$  and  $r_2$  accounting for atomic coherence were set to zero, thus modeling coherence loss, just prior to the application of the probe pulse. No difference in probe-pulse reshaping was observed between simulations including such coherence loss and those with a realistic coherence lifetime.

## 6. SUMMARY

This work has explored both experimentally and theoretically the excitation of inhomogeneously broadened, optically dense media by linear frequency-chirped optical pulses. A novel pump-probe technique was developed that sensitively identified average media half-inversion from the shape of a transmitted probe pulse. Maxwell-Bloch numerical modeling supports this association of the probe-pulse shape with media inversion, including the important case of half-inversion. A constant ratio of chirp intensity to chirp rate was observed experimentally to create a half-inversion on average through a medium of given optical density. Landau-Zener theory was shown to not only support this observation, but to imply that such a ratio is compactly contained in terms of a dimensionless coupling strength, and also to set a low optical-density bound on that ratio. Extensive Maxwell-Bloch modeling was used to both extend predictive capability into the optically dense regime and also to show agreement with Landau-Zener theory in the zero optical-density limit. Our work lays a foundation for utilizing chirped optical excitation in a precise and repeatable manner that is crucial for applications such as classical information storage and processing as well as quantum computation in rare-earth ion-doped solid-state materials.

## ACKNOWLEDGMENTS

The authors thank Scientific Materials Corporation for growing and preparing the crystal. We acknowledge many helpful discussions with R. L. Cone, Aleksander Re-

bane, and Y. Sun of the Physics Department at Montana State University; Tiejun Chang of The Spectrum Lab, Montana State University, for helpful discussions on Maxwell-Bloch numerical simulation; and Barry M. Garraway of the University of Sussex, UK, for useful correspondence. Robert Shelby, Ralph Devoe, Roger Macfarlane, and other members of the Quantum Metrology Group at the IBM Almaden Research Center were unstinting in giving their advice and support.

## REFERENCES AND NOTES

1. R. M. Macfarlane and R. M. Shelby, "Coherent transient and holeburning spectroscopy," in *Spectroscopy of Solids Containing Rare Earths*, A. A. Kaplyanski and R. M. Macfarlane, eds. (North-Holland, Amsterdam, 1987).
2. M. D. Levenson, "Time domain optical information storage in systems capable of photochemical hole burning," IBM Tech. Discl. Bull. **7**, 2797 (1981).
3. T. W. Mossberg, "Time-domain frequency-selective optical-data storage," Opt. Lett. **7**, 77-79 (1982).
4. J. R. Klauder, A. C. Price, S. Darlington, and W. J. Alberheim, "The theory and design of chirp radars," Bell Syst. Tech. J. **39**, 745 (1960).
5. Y. S. Bai and T. W. Mossberg, "Photon echo optical pulse compression," Appl. Phys. Lett. **45**, 1269-1272 (1984).
6. Y. S. Bai and T. W. Mossberg, "Experimental studies of photon-echo pulse compression," Opt. Lett. **11**, 30-32 (1986).
7. Y. S. Bai, W. R. Babbitt, and T. W. Mossberg, "Coherent transient optical pulse-shape storage recall using frequency-swept excitation pulses," Opt. Lett. **11**, 724-726 (1986).
8. T. Wang, H. Lin, and T. W. Mossberg, "Optical bit-rate conversion and bit-stream time-reversal by the use of swept-carrier frequency-selective optical-data storage techniques," Opt. Lett. **20**, 2033-2035 (1995).
9. K. D. Merkel and W. R. Babbitt, "Chirped-pulse programming of optical coherent transient true-time delays," Opt. Lett. **23**, 528-530 (1998).
10. R. W. Olson, H. W. H. Lee, F. G. Patterson, and M. D. Fayer, "Optical-density effects in photon-echo experiments," J. Chem. Phys. **76**, 31-39 (1982).
11. S. B. Altner, G. Zumofen, U. P. Wild, and M. Mitsunaga, "Photon-echo attenuation in rare-earth-ion-doped crystals," Phys. Rev. B **54**, 17493-17507 (1996).
12. M. Azadeh, C. S. Cornish, W. R. Babbitt, and L. Tsang, "Efficient photon echoes in optically thick media," Phys. Rev. A **57**, 4662-4668 (1998).
13. L. Allen and J. H. Eberly, *Optical Resonance and Two-Level Atoms* (Dover, New York, 1975).
14. N. Ohlsson, R. K. Mohan, and S. Kroll, "Quantum computer hardware based on rare-earth-ion-doped inorganic crystals," Opt. Commun. **201**, 71-77 (2002).
15. M. Nilsson, L. Levin, N. Ohlsson, T. Christiansson, and S. Kroll, "Initial experiments concerning quantum information processing in rare-earth-ion doped crystals," Phys. Scr. **T102**, 178-185 (2002).
16. L. D. Landau, "Zur Theorie der Energieübertragung II," Phys. Z. Sowjetunion **2**, 46 (1932).
17. C. Zener, "Non-adiabatic crossing of energy levels," Proc. R. Soc. London Ser. A **137**, 696 (1932).
18. N. V. Vitanov and B. M. Garraway, "Landau-Zener model: effects of finite coupling duration," Phys. Rev. A **53**, 4288 (1996).
19. For mathematical convenience, Vitanov and Garraway (Ref. 18) chose to define  $\Omega_0$  [rad/s] as half of the laboratory Rabi frequency on resonance and  $\beta^2$  [rad/s<sup>2</sup>] as half of the laboratory laser chirp rate, leading to a definition of the scaled dimensionless-coupling strength of  $\omega = \Omega_0/\beta$ . We have chosen quantities and units more convenient to the laboratory such that  $\Omega_0$  [s<sup>-1</sup>] is the full laboratory Rabi fre-



- quency of the chirp, and  $B_c/\tau_c$  [ $s^{-2}$ ] is the full laboratory chirp rate leading to definition of dimensionless-coupling strength given in Eq. (1). For comparisons with results in Ref. 26, it is easy to verify that  $\Phi = \omega/\sqrt{\pi}$ .
20. R. P. Feynman, F. L. Vernon, and R. W. Hellwarth, "Geometrical representation of the Schrodinger equation for solving maser problems," *J. Appl. Phys.* **28**, 49–52 (1957).
  21. R. Yano, M. Mitsunaga, and N. Uesugi, "Ultralong optical dephasing time in  $\text{Eu}^{3+}:\text{Y}_2\text{SiO}_5$ ," *Opt. Lett.* **16**, 1884–1886 (1991).
  22. R. W. Equall, Y. Sun, R. L. Cone, and R. M. Macfarlane, "Ultralow optical dephasing in  $\text{Eu}^{3+}:\text{Y}_2\text{SiO}_5$ ," *Phys. Rev. Lett.* **72**, 2179–2181 (1994).
  23. R. Yano, M. Mitsunaga, and N. Uesugi, "Nonlinear laser spectroscopy of  $\text{Eu}^{3+}:\text{Y}_2\text{SiO}_5$  and its application to time-domain optical memory," *J. Opt. Soc. Am. B* **9**, 992–997 (1992).
  24. F. Konz, Y. Sun, C. W. Thiel, R. L. Cone, R. W. Equall, R. L. Hutcheson, and R. M. Macfarlane, "Temperature and concentration dependence of optical dephasing, spectral hole lifetime, and anisotropic absorption in  $\text{Eu}^{3+}:\text{Y}_2\text{SiO}_5$ ," *Phys. Rev. B* **68**, 085109 (2003).
  25. Y. Sun, G. M. Wang, R. L. Cone, R. W. Equall, and M. J. M. Leask, "Symmetry considerations regarding light propagation and light polarization for coherent interactions with ions in crystals," *Phys. Rev. B* **62**, 15443–15451 (2000).
  26. B. A. Maximov, V. V. Illyukhin, Yu. A. Kharitonov, and N. V. Belov, "Crystal structure of yttrium oxyorthosilicate  $\text{Y}_2\text{O}_3 \cdot \text{SiO}_2 = \text{Y}_2\text{SiO}_5$  dual function of yttrium," *Sov. Phys. Crystallogr.* **15**, 806–812 (1971).
  27. C. Li, C. Wyon, and R. Moncorge, "Spectroscopic properties and fluorescence dynamics of  $\text{Er}^{3+}$  and  $\text{Yb}^{3+}$  in  $\text{Y}_2\text{SiO}_5$ ," *IEEE J. Quantum Electron.* **28**, 1209–1221 (1992).
  28. R. W. P. Drever, J. L. Hall, F. V. Kowalski, J. Hough, G. M. Ford, A. J. Munley, and H. Ward, *Appl. Phys. B* **31**, 97–105 (1983).
  29. R. L. Shoemaker, "Coherent transient infrared spectroscopy," in *Laser and Coherence Spectroscopy*, J. I. Steinfeld, ed. (Plenum, New York, 1978), pp. 197–317.
  30. Y. Sun, P. B. Sellin, C. M. Jefferson, and R. L. Cone, "Oscillator strength measurements on  $\text{Eu}^{3+}:\text{Y}_2\text{SiO}_5$ " (unpublished).
  31. A. E. Siegman, *Lasers* (University Science, Mill Valley, Calif., 1986).
  32. G. W. Burr, T. L. Harris, W. R. Babbitt, and C. M. Jefferson, "Incorporating excitation-induced dephasing into the Maxwell–Bloch numerical modeling of photon echoes," and references therein, *J. Lumin.* (to be published).